TWO DIMENSIONAL MAPPING OF ELECTRICAL PROPERTIES OF PV MODULES USING ELECTROLUMINESCENCE

Biao Li, Adam Stokes, Dan M. J. Doble
Fraunhofer Center for Sustainable Energy Systems
25 First Street Suite 101, Cambridge, MA, 02141, USA

ABSTRACT: Electroluminescence (EL) imaging has become an important quality control tool in maximizing module manufacturing yields through the detection of cracks in crystalline silicon cells. The technique offers the potential for collecting a 2D map of electrical properties of the cells since the intensity of individual pixels is related to the diode properties, series resistance and shunt resistance. However, determining such parameters analysis is complicated by the fact that pixel intensity is also affected by series resistance between the point and the metallization pattern. The work reported herein concerns a bias-dependant EL imaging technique that enables 2D spatial mapping of the electrical properties within cells and modules. Junction voltages and their difference among pixels have been derived from EL images at different bias. A distributed electrical model was then applied to fit the junction voltage change at each current and for each pixel, enabling acquisition of a 2D dark I-V curve for each point across the entire module. Cell parameters such as series resistance, shunt resistance, ideality factor and reverse saturation current can be extracted for each pixel. Following this, the light I-V equation was solved enabling the prediction of module performance under sun illumination.
Keywords: Electroluminescence, PV Module, Characterization

1 INTRODUCTION

For PV modules consisting of multiple cells, EL has been widely used as a qualitative instead of quantitative diagnosis tool. Challenges between EL image analysis of PV module versus single cell include the variation of optical and material properties of front encapsulant and/or cover glass in individual cells, additional resistance of the interconnection tabbing wires, additional contact resistance between the tabbing wire and cell, etc. All those cause the change of operating voltage as well as EL intensity of individual cell. Potthoff et al determined the operating voltage of individual solar cells in PV modules using the assumption that the highest EL signal is proportional to its operating voltage [1]. Weber et al distinguished between series and shunt resistance problems in a 2-cell mini-module in comparison with a reference cell using EL-based dark IV curves [2].

The main problem with EL is that the intensity of the images is governed not just by the electrical properties at a given point, but also by the series resistance between this point and the metallization [1]. It is therefore highly desirable to develop an effective approach capable of decoupling the series resistance effect. The work reported herein concerns a preliminary approach in this regard. A bias-dependant EL imaging technique has been developed that enables 2D spatial mapping of the electrical properties within cells and modules.

2 EXPERIMENTAL DETAILS

A mini-module was fabricated from six 6" multi-crystalline silicon cells connected in series and laminated with standard glass, EVA and backsheet materials. The module was placed in the dark room under current bias and an InGaAs camera (Xenics) with high quantum efficiency in 900 nm to 1700 nm range was utilized to record EL images. Constant current was applied to the module, and the voltage drop across the module was measured using a Keithley multimeter. EL images were acquired for each current increment of 0.1 A, starting with 0.1 A and ending with 8.6 A. A background image with zero current bias was subtracted from each image.

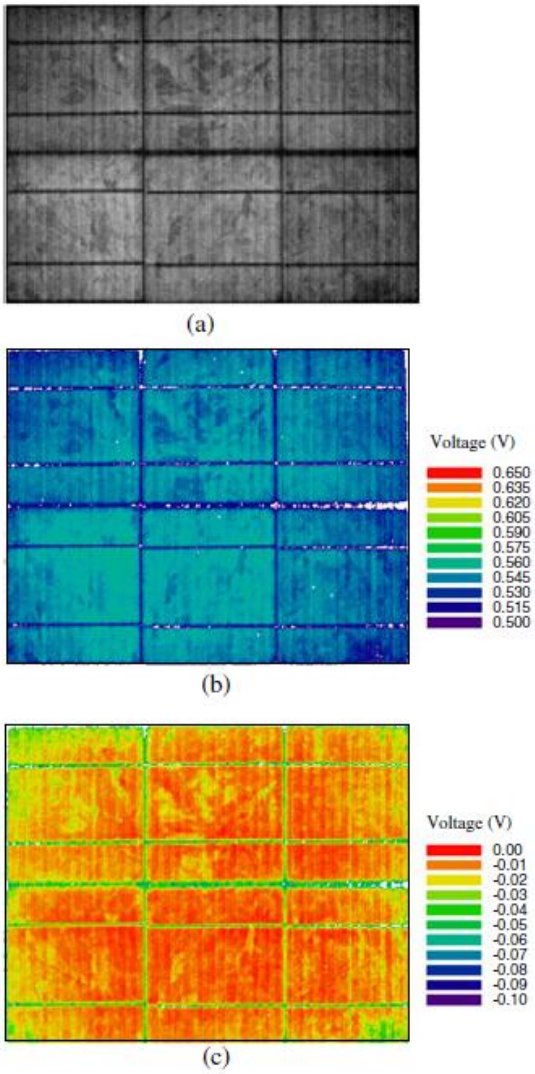

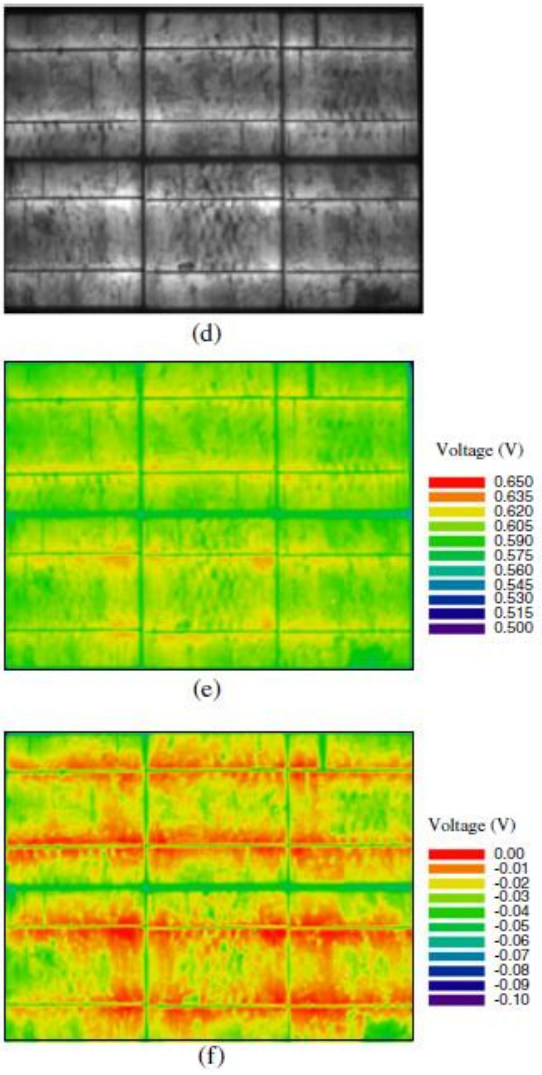

Figure 1: (a) EL image of the module at bias of 0.8 A. The pixel intensity is multiplied by 10. (b) Junction voltage of pixels at bias of 0.8 A; (c) Junction voltage difference among pixels of the PV module at bias of 0.8 A. (d) EL image of the module at bias of 8.5 A; (e) Junction voltage of pixels at bias of 8.5 A; (f) Junction voltage difference among pixels of the PV module at bias of 8.5 A.

In order to determine the junction voltage of each pixel from EL images, the scale factor was first derived from the EL image under low current conditions, typically less than 0.1·Isc, according to Ref [1]. We also make the same assumption as in Ref [1] that the highest EL intensity in each image corresponds to zero internal series resistance. The junction voltage difference, dV, between pixels can then be calculated with reference to the brightest pixel. Figure 1 shows EL images, junction voltage of pixels, and junction voltage difference among pixels of the PV module at 0.8 A and 8.5 A, respectively. The junction voltage difference between pixels is seen to increase with increasing bias current as is to be expected since the voltage drop between pixels is equal to the bias current multiplied by the series resistance [1].

3 BIAS-DEPENDENT EL ANALYSIS

A distributed series resistance model has been developed elsewhere to analyze current density, J_{meas}, and voltage characteristics measured at the terminals of the module [3]. We utilized a similar model to evaluate the junction voltage V_{EL} at different current density J_{meas}. The diode current density J_{EL} and the shunt current density J_{sh} depend on the local diode voltage V_{EL} (Figure 2a). The difference of diode current between any pixel, J_{EL}, and the brightest pixel, J_{meas}, is assumed to be proportional to the difference of junction voltage between them, dV(i,j). Signs for current and voltage are chosen to be positive for the device operating as an active solar cell. For any pixel located at i-column and j-row, we have

$$J_{meas} = J_0(i,j) \cdot exp\left(\frac{V_{EL}(i,j)}{n(i,j)\cdot V_T}\right) + \frac{V_{EL}(i,j)}{R_{sh}(i,j)} + C \cdot dV(i,j) \qquad (1)$$

where $J_0(i,j)$, $n(i,j)$, and $R_{sh}(i,j)$ are reverse saturation current density, ideality factor, and shunt resistance, respectively, for pixel (i,j) in EL images. V_T is the thermal voltage, and C the fitting parameter. Providing $V_{EL}(i,j)$ and dV(i,j) from bias-dependant EL, the cell parameters can be evaluated. Figure 2b represents the measured and fitted J_{meas}-V_{EL} profile for one pixel.

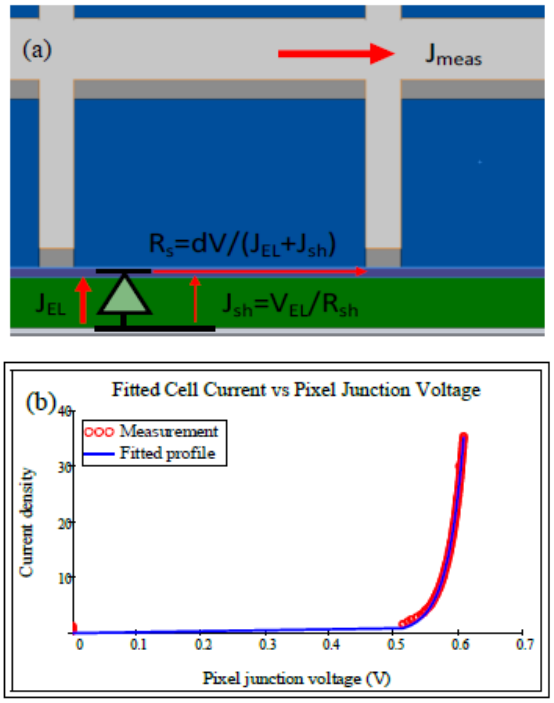

Figure 2: (a) Distributed electrical model for EL imaging analysis. The diode current density J_{EL} and the shunt current density J_{sh} depend on the local diode voltage V_{EL}. Sheet resistance is evaluated as the ratio of pixel voltage difference, dV, to the sum of J_{EL} and J_{sh}. (b) Measured and fitted J_{meas}-V_{EL} profiles for the (i,j) pixel with junction voltage $V_{EL}(i,j)$.

Based on the fitting parameters, the distributed series resistance R_s can be calculated as the ratio of dV(i,j) to the sum of $J_{EL}(i,j)$ and $J_{sh}(i,j)$ for any pixel. Contributions to R_s include sheet resistivity of the n-layer, distributed metallic resistance along a grid line or busbar etc [3]. Figure 3 illustrates the calculated series resistance for a pixel. R_s

decreases with increasing junction voltage. This is consistent with the trend observed elsewhere that R_s decreases slightly with increasing injection level [4].

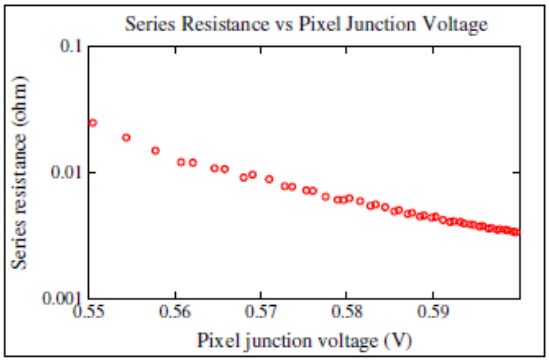

Figure 3: Calculated series resistance of a pixel as a function of pixel voltage $V_{EL}(i,j)$.

Figures 4a-d display the 2D distribution of series resistance, shunt resistance, reverse saturation current and ideality factor across the module derived from bias-dependant EL images. Inactive regions in the module, i.e. busbars and gap between cells can be distinguished. With the ability of acquiring a 2D map of cell and module electrical properties, this technique has promise for identifying material or process related failures such as large series resistance and shunts.

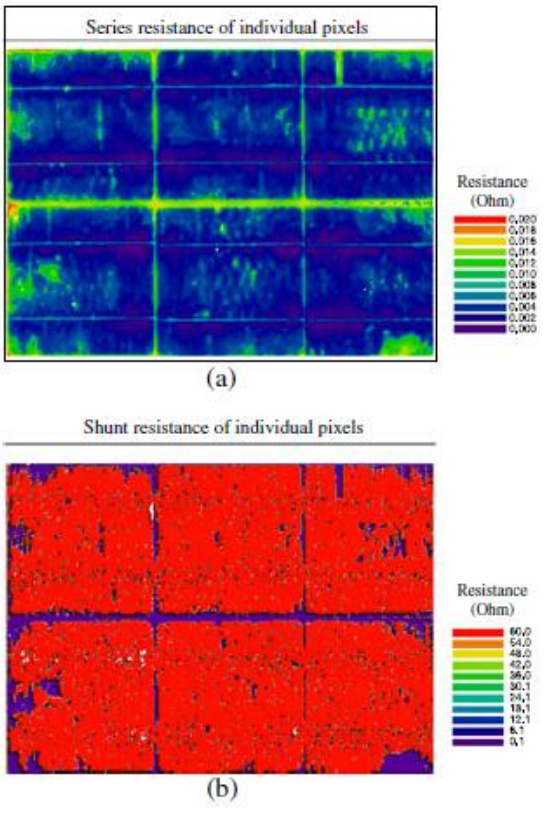

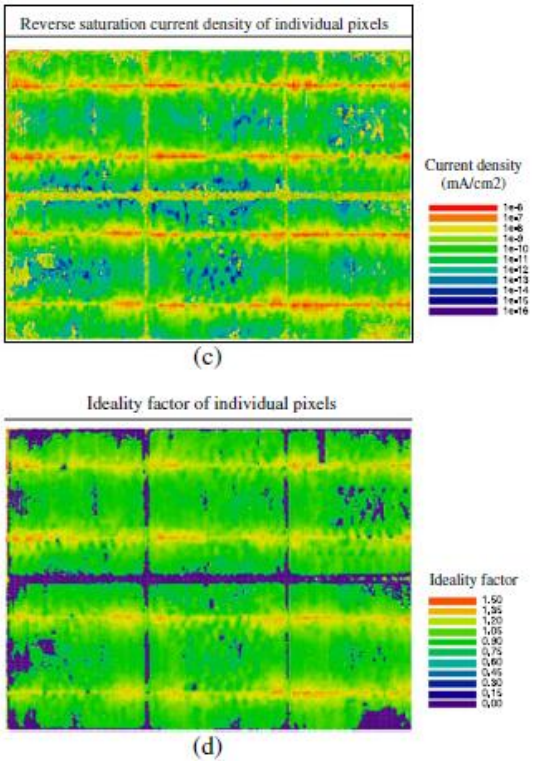

Figure 4: 2D distribution of (a) series resistance, (b) shunt resistance, (c) reverse saturation current density, and (d) ideality factor, across the module derived from bias-dependant EL images.

We further utilized a simple lumped electrical model to predict the module performance under illumination based on the cell parameters determined from bias-dependant EL. For a one-diode electrical model, the photo-generated current density is expressed as

$$J = J_L - J_0 \cdot \exp\left(\frac{V+J\cdot R_s}{V_T}\right) - \frac{V+J\cdot R_s}{R_{sh}} \qquad (2)$$

This is a transcendental equation which is typically solved using graphical or numerical methods. However, we have developed a solution to Eq. (2) in closed form using Lambert W Function [5]. The contribution of individual pixel to photo-generated current at certain voltage can be expressed as:

$$J = \frac{J_0(i,j)R_{sh}(i,j) - V + I_{ph}R_{sh}(i,j)}{R_s(i,j)+R_{sh}(i,j)} - \frac{V_T n(i,j)}{R_s(i,j)} * W\left[\frac{I_0(i,j)R_s(i,j)R_{sh}(i,j)\exp\left(\frac{1.16\times10^4 R_{sh}(i,j)\left(V+I_0(i,j)R_s(i,j)+I_{ph}R_s(i,j)\right)}{T\cdot n(i,j)\left[R_s(i,j)+R_{sh}(i,j)\right]}\right)}{V_T n(i,j)\left(R_s(i,j)+R_{sh}(i,j)\right)}\right] \qquad (3)$$

By prescribing a value for light generated current density J_L and inserting the parameters shown in pixel resolution in Figure 4 into Eq. (3), the contributions of individual pixel to open circuit voltage, short circuit current, voltage and current at maximum power point (MPP) under illumination can be predicted. For our module with 6 cells connected in series, the distribution of array voltage at open circuit and MPP conditions can also be calculated.

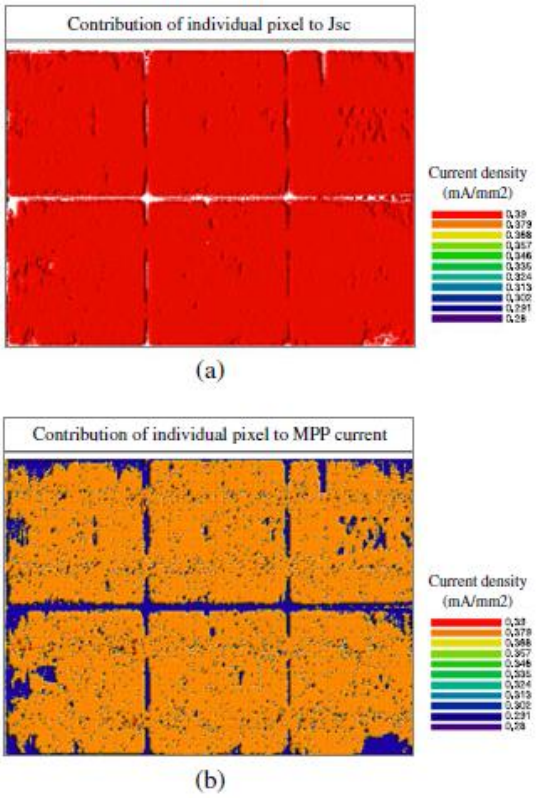

Figure 5: Contribution of individual pixel to module current density at (a) short circuit and (b) MPP conditions, respectively, for the module with 6 cells connected in series.

Figure 5 shows the expected current density generated at each pixel under short circuit conditions. Despite the non-uniformity in the EL, the current density is for the most part uniform across the pixels in the module. This is because J_{sc} is mainly associated with light absorption properties of each pixel as well as carrier separation capability of the internal electrical field, both are assumed to be uniform across the absorber areas of the module. Under MPP conditions, the non-uniformity in the current contributions from the pixels is more apparent. This is rationalized in terms of the increase in internal current flow in areas of low internal shunt resistance when an external load is applied. The similarities between the MPP generated current (Figure 5b) and the shunt resistance maps (Figure 4b) support this rationalization.

Figure 6a and b exhibit the predicted voltage generated at each pixel under open circuit and MPP conditions, respectively. In contrast to the short circuit current, the contribution of individual pixels to open circuit voltage varies significantly for different pixels with the highest voltages seen next to bus-bars. This reflects the fact that V_{oc} is related to the ratio J_{sc} and $J_0(i,j)$ at each pixel. Thus, Figure 6a is close to the combination of Figure 5a and Figure 3c. At MPP condition, pixels with large reverse saturation current and low shunt resistance result in the current flowing internally within the pixel rather than contributing to the external current.

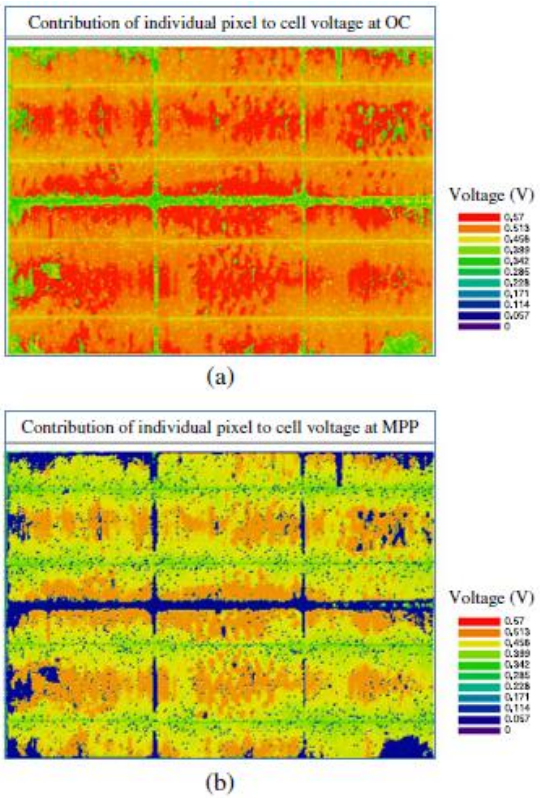

Figure 6: Contribution of individual pixel to cell voltage at (a) open circuit and (b) MPP conditions, respectively.

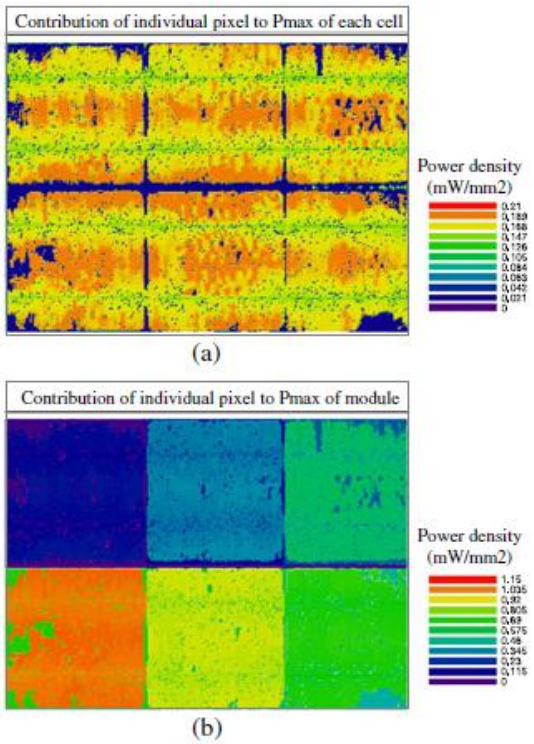

Figure 7: Contribution of individual pixel to maximum power output of (a) individual cell, and (b) entire module, respectively.

Figure 7a and b show the predicted power generated at each pixel for individual cell and entire module, respectively, under MPP condition. For the test module with 6 cells connected in series, the voltage difference between neighboring cells is assumed to be 0.46 V at MPP condition according to light I-V measurement. The absolute voltage generated at each pixel of different cells was then estimated. Combining with the results in Figure 5b, the contribution of individual pixel to maximum power output was mapped out (Figure 7). The individual cell power does not show much distinction. The feature in Figure 7a can be reconstructed by a combination of the V_{mp} image (Figure 6b) and the I_{mp} image (Figure 5b). As for the module (Figure 7b), the operating voltage builds up gradually from the top left to the top right cells and then from the bottom right to the bottom left cells. As a result, the V_{mp} features in individual cells (Figure 6b) are dampened. However, the total current remains the same for each cell. Thus the I_{mp} features in individual cells remain. It is clear that the pixels with defects contribute less module power to the load than the good ones.

4 CONCLUSION

In summary an approach has been developed to evaluate a 2D map of electrical properties across a module. This approach is equivalent to generating a 2D map of dark I-V curves across the entire module and enables evaluation of series resistance, shunt resistance, ideality factor and reverse saturation current at each pixel. These parameters can be substituted into the solution of light I-V equation to enable the performance of the module under illumination to be predicted.

References

[1] T. Potthoff, K. Bothe, U. Eitner, D. Hinken, M. Kontges, Prog. Photovolt: Res. Appl., 18 (2010) 100

[2] T. Weber, M. Kutzer, Proceedings of 24th European Photovoltaic Solar Energy Conference (2009) 477

[3] L. Nielsen, IEEE Transactions on Electron Devices, ED29 (1982) 821

[4] A. Aberle, S. Wenham, M. Green, Proceedings of 23rd IEEE Photovoltaic Specialists Conference, (1993) 133

[5] R. Corless, G. Gonnet, D. Hare, D. Jeffrey, D. Knuth, Advances in Computational Mathematics 5 (1996) 329